Published March 12, 2024 as 10.3174/ajnr.A8245

ORIGINAL RESEARCH

Neurodegenerative Disorder Imaging

Individual Structural Covariance Network Predicts Long-Term Motor Improvement in Parkinson's Disease with STN-DBS

Yu Diao, MD,[1†] Hutao Xie, MD,[1] Yanwen Wang, MD. PhD[1], Baotian Zhao, MD. PhD[1], Anchao Yang, MD. PhD,[1,2] Jianguo Zhang, MD, PhD,[1,2*]

ABSTRACT

BACKGROUND AND PURPOSE: The efficacy of long-term chronic subthalamic nucleus deep brain stimulation (STN-DBS) in treating Parkinson's Disease (PD) exhibits substantial variability among individuals. The preoperative identification of suitable DBS candidates through predictive means becomes crucial. Our study aims to investigate the predictive value of characterizing individualized structural covariance networks for long-term efficacy of DBS, offering patients a precise and cost-effective preoperative screening tool.

MATERIALS AND METHODS: We included 138 PD patients and 40 healthy controls. We developed individualized structural covariance networks from T1-weighted images utilizing Network Template Perturbation, and computed the networks' topological characteristics. Patients were categorized according to their long-term motor improvement following STN-DBS. Intergroup analyses were conducted on individual network edges and topological indices, alongside correlation analyses with long-term outcomes for the entire patient cohort. Finally, machine learning (ML) algorithms were employed for regression and classification to predict post-DBS motor improvement.

RESULTS: Among the PD patients, six edges (left Middle Frontal and left Caudate Nucleus, right Olfactory and right Insula, left Superior Medial Frontal Gyrus and right Insula, right Middle Frontal and left Paracentral Lobule, right Middle Frontal and Cerebellum, left Lobule VIIb of the Cerebellum and the vermis of the Cerebellum) exhibited significant results in intergroup comparisons and correlation analyses. Increased degree centrality and local efficiency of the cerebellum, parahippocampal gyrus, and postcentral gyrus were associated with DBS improvement. A regression model constructed from these six edges revealed a significant correlation between predicted and observed changes in the unified Parkinson's disease rating scale ($R=0.671$, $P<0.001$), and receiver operating characteristic analysis demonstrated an area under the curve of 0.802, effectively distinguishing between patients with good and moderate improvement post-DBS.

CONCLUSIONS: Our findings reveal the link between individual structural covariance network fingerprints in PD patients and long-term motor outcome following STN-DBS. Additionally, binary and continuous cerebellum-basal ganglia-frontal structural covariance network edges have emerged as potential predictive biomarkers for DBS motor outcome.

ABBREVIATIONS: subthalamic nucleus deep brain stimulation = STN-DBS; Parkinson's Disease = PD; machine learning = ML); Network Template Perturbation = NTP.

Received month day, year; accepted after revision month day, year.
From the Department of Neurosurgery, Beijing Tiantan Hospital, Capital Medical University, Beijing, China (Y.D, H.X, Y.W, B.Z, A.Y, J.Z), and Beijing Key Laboratory of Neurostimulation, Beijing, China (A.Y, J.Z).

The authors declare no conflicts of interest related to the content of this article.

Please address correspondence to Prof. Jianguo Zhang. Capital Medical University, Department of Functional Neurosurgery, Tiantan Hospital, No. 119 South 4th Ring West Road, Fengtai District, 100070, Beijing, China. e-mail- zjguo73@126.com.

SUMMARY SECTION

PREVIOUS LITERATURE: The effectiveness of long-term STN-DBS in treating PD varies significantly among individuals. The preoperative identification of suitable DBS candidates through predictive methods becomes imperative. The clinically utilized dopamine challenge test demonstrates limited efficacy in predicting long-term outcomes. With the recognition of aberrant characteristics in the whole-brain networks in PD, individual brain networks constructed based on fMRI are used for postoperative predictions. However, the extended scan duration, notable variability, and economic constraints associated with fMRI restrict its applicability and practicality. Therefore, there is a clinical need for predictive methods that exhibit both robust efficacy and economic feasibility.

KEY FINDINGS: Binary and continuous structural covariance network edges linking the cerebellum, basal ganglia, and frontal regions have emerged as potential predictive biomarkers for the motor outcome of DBS.

KNOWLEDGE ADVANCEMENT: This study contributes to providing an economically viable and objectively convenient predictive tool for identifying suitable candidates for DBS.

Copyright 2024 by American Society of Neuroradiology.

INTRODUCTION

Deep brain stimulation of the subthalamic nucleus (STN-DBS) is an effective therapy for improving long-term motor symptoms in patients with Parkinson's disease (PD) [1, 2]. However, the long-term effectiveness of DBS relies on preoperative patient selection, precise targeting during implantation, postoperative programming, and ongoing medicine management [3]. Long-term STN-DBS can lead to the motor and cognitive complications in some patients [4], and there is considerable individual variation in the postoperative improvement of motor symptoms [5, 6]. Therefore, identifying effective predictive factors preoperatively is crucial for patient selection.

In many DBS centers, Levodopa Challenge Test (LCT) serves as a critical predictor for evaluating the motor prognosis of DBS [7, 8]. While LCT proves effective in identifying patients with a non-responsive reaction to levodopa, its predictive accuracy for postoperative long-term motor outcomes exhibits significant variability and lacks precision [7-10]. Additionally, the emotional burden induced by the Med-OFF state and the hospital environment can lead to inaccuracies in the LCT results [11]. Existing research suggests that the modulation of motor symptoms in PD patients through STN-DBS is based on the regulation of large-scale brain networks [12, 13]. Due to the dynamic time characteristics of fMRI [14], individual brain networks constructed based on fMRI are increasingly employed for postoperative prediction [15, 16]. However, noise sources such as physiological factors (e.g., motion, respiration), miscellaneous non-physiological factors (e.g., scanner drift), coupled with the several minutes scans, contribute to significant variability in fMRI [17]. Additionally, economic constraints associated with fMRI also limit its applicability and value. All above potentially render it unsuitable for all DBS centers. Given these challenges, there is a pressing need for a more objective and stable postoperative prediction method. The advantages of T1 scans include shorter scan times, minimal sensitivity to physiological influences, and controlled error within 2% in repeated scans on the same equipment, demonstrating the stability of its scan results [18, 19]. T1 scans are a routine sequence in many centers, offering economic advantages as well. The latest Network Template Perturbation (NTP) methods [20] have facilitated the construction of structural covariance networks. The predictive potential of brain networks for long-term motor outcomes, investigated in fMRI research, may also be attainable by depicting brain networks using structural covariance.

In previous studies, the relationship between T1-based brain morphometry and long-term therapeutic outcomes has been established [21]. Gray matter atrophy in the frontal lobe [22] and precentral cortex [23] have also shown effective predictive relationships with long-term motor response. Additionally, in PD patients, damage to the structural covariance network (SCN) from the basal ganglia to regions such as the sensorimotor cortex has been observed based on T1-weighted images at the group level[24, 25]. However, group-based SCNs often overlook individual differences and fail to uncover the relationship between brain structural networks arising from individual variability and improvements in clinical symptoms. In this study, we employed NTP, based on T1, to construct individualized structural covariance networks (ISCN) and investigate the predictive value of ISCN for long-term motor improvement following STN-DBS [20]. This approach allowed us to explore the heterogeneity of structural covariance networks at the individual level.

In this study, the network edge selection was determined based on correlations with long-term prognosis and between-group comparisons. Graph theory analysis was utilized to identify nodes in the network crucial for long-term outcome. Ultimately, machine learning (ML) techniques were employed to predict the extent of motor improvement in PD patients after STN-DBS.

MATERIALS AND METHODS

Study Design and Participants

The study retrospectively included patients from 2016 to 2022 at Beijing Tiantan Hospital, Capital Medical University, China. Inclusion criteria are: (1) diagnosed with idiopathic PD [26]; (2) patients underwent bilateral STN-DBS; (3) completing motor and non-motor assessments at baseline and at least 1 year post-surgery; (4) meeting quality control standards on neuroimaging examination. Age matched HCs were individuals aged between 40-80 years without any neurological disorders. Ultimately, a total of 138 PD patients were retrospectively included, with 40 HCs. Baseline information is summarized in Table 1.

Clinical Examinations

Detailed clinical assessments included Movement Disorder Society-sponsored Unified Parkinson's Disease Rating Scale (MDS-UPDRS), Berg balance scale (Berg) and freezing of gait questionnaire (FOG-Q), Montreal cognitive assessment (MoCA), Hamilton Anxiety Rating Scale (HAMA) and Hamilton Depression Rating Scale (HAMD). These clinical assessments were conducted by two movement disorder experts within the first two weeks preceding DBS, during both the medication-off (Med-OFF) and medication-on (Med-ON) states. The Med-OFF state was defined as abstaining from antiparkinsonian drugs for at least 12 hours, while the Med-ON state was defined as having taken antiparkinsonian drugs for at least 1 hour. The levodopa equivalent daily dose (LEDD) for each patient's antiparkinsonian drugs is detailed in Table 1 [27]. Follow-up assessments were conducted at 1-3 years post-surgery in both stimulation-on (Stim-ON)/Med-ON and Stim-ON/Med-OFF states. The specific surgical procedure and follow-up protocol can be found in the supplementary materials.

The impact of DBS on clinical motor improvement was quantified as a percentage improvement on the MDS-UPDRS-III. MDS-UPDRS-III consists of 33 scores derived from 18 items, with each item scored on a scale of 0 to 4. A score of 0 indicates normalcy, while a score of 4 signifies severe impairment [28]. The improvement percentage of DBS was further used to categorize patients into good improvement group (GIG) and moderate improvement groups (MIG). The formula for calculating the improvement percentage is as follows:

$$(\text{preoperative UPDRS\_III(Med OFF)} - \text{postoperative UPDRS\_III(Med OFF/Stim ON)}/\text{ preoperative UPDRS\_III(Med OFF)})$$

Previous studies have indicated that patients undergoing STN-DBS with an improvement rate exceeding 30% are considered to exhibit a beneficial response to stimulation [11]. Therefore, we defined the MIG as patients with an improvement rate of 30% or less. Additionally,

the confidence interval for the overall maximum improvement in UPDRS ranges from 69.8 to 45.8 [29]. Therefore, patients with an improvement rate of 70% or higher were categorized as the GIG. In the group analysis, only patients with DBS improvement rates below 30% and above 70% were included. This was done to enhance sensitivity in the analysis. Detailed information on patient grouping based on DBS improvement rates is shown in Figure 2 and Table S1.

All post-operative images of the patients were reviewed to confirm the absence of electrode displacement. The final follow-up stimulation parameters for both patient groups were comparable (Table S2 and S3).

Individual Differential Structural Covariance Network (IDSCN) Measures

As the conventional group-level SCN analysis tends to lose individualized network information, we adopted a recently established method, NTP, as outlined by Liu, Z et al [20], to construct individual-specific SCN networks. Details of T1 data acquisition and preprocessing can be found in the supplementary materials.

Specifically, we followed the steps depicted in Figure 1. Initially, a reference SCN was constructed within the HC group (n = 40). This network was generated by calculating the partial Pearson correlation coefficient (PCC) between gray matter volumes of each pair of brain regions, while considering total intracranial volume (TIV) as a covariate and denoted as PCCn. Subsequently, every patient was introduced into the HC group, resulting in n + 1 subjects (n controls and 1 patient), and a new structural covariance network termed the perturbed network PCCn+1 was constructed. Calculation of the difference between the perturbed network and the reference network, ΔPCCn = PCCn+1 – PCCn, followed. Lastly, given that ΔPCCn exhibited a novel symmetrical distribution known as the "volcano distribution" [30], we computed the Z-score for ΔPCCn using a Z-test as followed:

$$Z = \frac{\Delta PCCn}{\frac{1-PCC_n^2}{n-1}}$$

The IDSCN network for every patient was subsequently constructed, where the weight of each edge was determined by the Z-scores obtained from the Z-test. Moreover, we calculated the P value for each edge in the IDSCN network for every patient based on the Z-score. Finally, we identified edges in each patient's IDSCN that significantly deviated from the reference network, applying Bonferroni correction. The edges within the IDSCN convey how the inclusion of an additional patient altered the covariance of gray-matter volume pairs for specific brain regions compared to the reference group. Ultimately, for each patient, we constructed IDSCN consisting of 12,090 edges, based on 156 brain regions defined by the AAL3 atlas (Table S4). The edges in the IDSCN represent how the covariance between two brain regions in an individual patient deviates from the reference structural covariance network observed in HCs.

Network analysis

We selected a range of sparsity thresholds (K = 0.14 ~ 0.5, with an increment of 0.01) to binarize the IDSCN and computed global and nodal network topological properties. Global metrics (small-world attributes and global efficiency) and node-level metrics (degree centrality, local efficiency) were computed were calculated using the GRETNA software package [31]. Definition of graph theory metrics can be found in supplementary materials.

For each sparsity threshold, network metrics were calculated, and quantitative analysis of graph theoretical metrics was performed by computing the Area Under the Curve (AUC) within the entire sparsity range.

Patients splitting and Multi-Layer Perceptron classification

We selected the top 5% of edges based on their Z-scores for subsequent analysis [20]. This approach was employed to ensure that such differences would not be confounded by an excessive number of nodes and edges in further inter-group analysis and predictive model construction. Firstly, we assessed whether there existed group-level differences in network properties, which could serve as indicators of long-term prognosis. We divided the dataset into training/validation (a set) and testing (b set) sets in a 7.5:2.5 ratio. Within a set, we ranked the edges based on their correlation with the DBS improvement and considered the absolute values. Additionally, covariates such as age, gender, Total Intracranial Volume (TIV), and MoCA scores were taken into account. We selected the top 1% of the correlated edges from a set, resulting in six edges (n=6). Subsequently, we conducted group-wise comparisons between these six edges in the overall groups.

Next, we employed a Multi-Layer Perceptron Classifier (neural network) with default parameters from scikit-learn on the top 1% correlated edges in a set [32]. This evaluation aimed to assess the model's ability to differentiate the responsiveness to STN-DBS based on combinations of network edges. We performed 5-fold cross-validation on a set to test the model's performance. Finally, the model was evaluated on b set. This involved generating Receiver Operating Characteristic (ROC) curves on b set, plotting the True Positive Rate (TPR) against the False Positive Rate (FPR). The performance of the tested model was quantified by calculating the AUC of the average ROC curve.

STN-DBS outcome prediction using XGBoost

We utilized XGBoost to investigate whether preoperative network fingerprints can predict the long-term DBS efficacy for all patients. Initially, we divided the dataset into training/validation and testing sets in a 75%:25% ratio, followed by feature selection within the training/validation set where we chose the top 1% of edges. Subsequently, data standardization was performed. Through grid search, we determined the optimal hyperparameter combination for the XGBoost regression model, including n_estimators (the number of base learners) and learning_rate (the weight shrinkage of each base learner). During the hyperparameter search, we experimented with different values to find the best combination. For n_estimators, we explored a range from 10 to 200, while for learning_rate, we explored a range from 0.01 to 0.1.

Following this, we trained the XGBoost regression model on the training dataset using the best hyperparameter combination and evaluated its performance through five-fold cross-validation on the training/validation dataset to assess hyperparameter performance. Subsequently, we assessed the model's performance by predicting long-term DBS improvement on the testing dataset. To compute feature importance, we utilized the built-in feature_importances attribute of the XGBoost library, providing the relative importance of each feature in predicting the model. Evaluation metrics included the correlation coefficient between predicted and actual values, offering insights into the model's predictive accuracy. Additionally, we computed the mean squared error (MSE) as a quantifiable measure of overall prediction error.

Statistical Analyses

The comparison of changes in outcomes from baseline to long-term follow-up for all patients, which did not conform to a normal distribution, was assessed using Wilcoxon signed-rank tests. Following grouping into GIG, MIG, and HC, an analysis of variance (ANOVA) was employed to examine age and gender differences among the groups. Comparisons between the GIG and MIG groups underwent a normality test, and if the data followed a normal distribution, a two-sample t-test was applied. Non-normally distributed data were analyzed using Mann-Whitney U-tests. All results are presented as mean ± standard deviation, and statistical significance was defined as $p<0.05$.

Inter-group differences in gray matter network connectivity were evaluated using ANCOVA tests, with age, gender, TIV, and MoCA scores as covariates. Multiple comparisons were corrected using the False Discovery Rate (FDR), and FDR-adjusted p-values (FDR p) below 0.05 were considered statistically significant. The correlation between gray matter volume network edges and long-term improvement in DBS was assessed using Partial correlation analysis with age, gender, TIV, and MoCA scores as covariates.

RESULTS

Clinical characteristics

40 HCs and 138 PD patients with complete long-term follow-up assessments were screened for inclusion. The median follow-up time was 3 years (confidence interval 2.78-3.11). The average age of PD patients was 62.08 ± 8.52 years, with an average disease duration of 11.72 ± 4.73 years.

PD patients exhibited a significant reduction in MDS-UPDRS-III scores, decreasing from an average of 49.86 to 24.61 following long-term STN-DBS ($P<0.001$). Furthermore, tremor and rigidity scores showed significant improvement ($P<0.001$). Other results can be found in Table 1.

As indicated in Table S2, there were no significant differences observed among the GIG, MIG, and HC groups in terms of age ($P = 0.768$) and gender ($P = 0.327$). Additionally, there were no significant differences between the two patient groups in terms of UPDRS improvement rates during preoperative levodopa responsiveness testing ($P = 0.854$) and disease duration ($P = 0.452$). The long-term therapeutic effects on both motor and non-motor symptoms for the two patient groups are presented in Figure 2. Patients in the GIG who exhibited significant improvement in UPDRS-III scores also demonstrated more pronounced improvements in HAMA, Berg, and FOG-Q.

Preoperative Grey Matter and Network Fingerprints

The volume of gray matter did not exhibit significant differences between the two groups. In comparison to the GIG group, the MIG group showed significantly increased connectivity Z-scores for the connection between the left Middle Frontal Gyrus (Frontal_Mid_2_L) and the left Caudate nucleus (Caudate_L) (FDR $p = 0.013$), the right Olfactory Cortex (Olfactory_R) and the right Insula (Insula_R) (FDR $p = 0.020$), the left Superior Medial Frontal Gyrus (Frontal_Sup_Medial_L) and Insula_R (FDR $p = 0.020$), the right Superior Frontal Gyrus (Frontal_Sup_2_R) and the left Paracentral Lobule (Paracentral_Lobule_L) (FDR $p = 0.009$), the right Middle Frontal Gyrus (Frontal_Mid_2_R) and the right Crus II of the Cerebellum (Cerebellum_Crus2_R) (FDR $p = 0.009$), and the left Lobule VIIb of the Cerebellum (Cerebellum_7b_L) and the vermis of the Cerebellum (Vermis_6) (FDR p = FDR $p = 0.009$). Detailed results are shown in Figure 3.

Post-operative images of both patient groups were examined, and no electrode displacement was observed. No significant differences in stimulation parameters were found between the two groups (Table 3). The six edges demonstrated good predictive capabilities for long-term efficacy, achieving a maximum AUC area of 0.802 when employing the Multi-Layer Perceptron Classifier (Fig 3B).

Relationship of Network Topologies and DBS Outcomes

We found that global properties showed no significant correlation with long-term DBS outcomes. However, degree centrality and local efficiency exhibited significant correlations with long-term DBS prognosis. The degree centrality of the right Middle Cingulate Cortex (rMCC) (FDR $p = 0.015$), left Parahippocampal Gyrus (lPHG) (FDR $p = 0.025$), right Postcentral Gyrus (rPoCG) (FDR $p = 0.034$), and Vermis 4-5 (VER4_5) (FDR $p = 0.011$) demonstrated a positive correlation with long-term DBS improvement. Additionally, among the local efficiency, the left Parahippocampal Gyrus (lPHG) ($P = 0.048$), right Parahippocampal Gyrus (rPHG) ($P = 0.040$), right Postcentral Gyrus (rPoCG) ($P = 0.024$), left Supramarginal Gyrus (lSMG) ($P = 0.030$), and left Lobule 3 of the Cerebellum (lCER3) ($P = 0.033$) exhibited positive correlations with long-term prognosis. Detailed results are presented in Figure 4, Table S5, and S6.

Predictors of STN-DBS Responsiveness

When age, gender, TIV were considered as covariates, the correlations between the top 1% ranked network edges and DBS improvement rates are depicted in Figure 5. When testing the predictive performance of gray matter volume Network Fingerprints for long-term efficacy using XGBoost in the test dataset, the correlation between actual values and predicted values was 0.671, with an MSE of 0.055, showed in Figure 5B. The most significant contribution is represented by edge 'Frontal_Sup_Medial_L' and 'Insula_R' (0.428).

DISCUSSION

This study investigated the impact of STN-DBS on long-term motor improvement in PD patients. The observation revealed that patients with more favorable DBS improvement displayed IDSCN characteristics and network topological attributes that closely resembled those of healthy individuals. Additionally, potential outcome predictors were examined, revealing that IDSCN fingerprints could predict the long-term improvement outcomes of DBS.

The absence of a significant difference in preoperative levodopa responsiveness between the GIG and MIG groups validates previous findings that levodopa responsiveness alone is not a reliable predictor of long-term DBS outcomes [7, 33]. We did not observe significant differences between the two patient groups in terms of stimulation parameters, despite it being recognized as important determinants of long-term postoperative efficacy [34]. During the chronic DBS phase following multiple programming adjustments, suboptimal outcomes were still evident in some late-stage PD patients [35]. This underscores the substantial challenge of accurately selecting appropriate candidates for DBS therapy [36]. Intriguingly, we did not detect differences in gray matter volume within individual brain regions between the two patient groups; rather, differences were observed exclusively within the gray matter network. This suggests that long-term efficacy in these patients may be more influenced by network characteristics rather than structural abnormalities within isolated brain regions.

The correlation analysis between the topological properties and long-term clinical outcomes revealed that parahippocampal area, postcentral gyrus, and supramarginal gyrus, as well as the cerebellum, exhibited nodal local efficiency and degree centrality positively corelated with improved long-term outcomes. These regions are implicated in spatial cognition and motor coordination [37], with previous cortical structural studies reporting atrophy in these areas among PD patients [38]. While we did not validate our findings with an external dataset, our results align with previous research, particularly in the comparison of PD to HC. PD patients exhibit a disrupted topological organization of cortical morphological networks with a significant decline in local efficiency [39]. Our results suggest a network with greater structural integration and reduced isolation, might be more susceptible to modulation by DBS. This observation aligns with previous research findings that indicate DBS exerts widespread regulatory effects on functional connectivity within cortical regions [15].

Notably, the abnormal motor-cognitive gray matter network fingerprint identified in this study may serve as one of the key explanations for the observed long-term efficacy disparities. These network aberrations primarily stem from reconfigurations within the motor-cognitive network, such as alterations between the frontal cortex and cerebellum, the caudate nucleus, as well as the frontal cortex and the paracentral lobule (PCL). The role of frontal lobe function and structural abnormalities in influencing the long-term motor efficacy of DBS stimulation has been elucidated in PD patients [3, 22, 40]. The cerebellum-basal ganglia-frontal network aberrations play a pivotal role in the motor coordination and control deficits observed in PD patients [41]. The frontal cortical function may deteriorate in response to high-frequency STN-DBS stimulation, exacerbating patients' motor coordination and cognitive abilities [42]. Our research findings indicate that structural co-variation connections between the cerebellum, frontal cortex, and caudate nucleus have predictive value for the motor outcomes of DBS, providing evidence for the necessity of higher-level cognitive network control in motor coordination. Indeed, as demonstrated by some studies, PD patients with more severe caudate nucleus damage [43] and lower frontal lobe scores [3] tend to exhibit poorer long-term motor prognosis.

To date, despite an abundance of studies elucidating potential determinants of long-term outcomes following DBS, the majority of investigations have centered around preoperative assessments, such as gait scores [44], postural stability [35], and frontal scores [3]. However, these scales required substantial time and personnel, and their susceptibility to the vagaries of subjective assessments by clinicians and the influence of patients' anxious states in the clinical setting [45]. In contrast, the motor-cognitive gray matter network fingerprint remains impervious to emotional factors and variations in the expertise of clinicians. In a broader context, the characteristics of the preoperative motor-cognitive gray matter network fingerprint may be indicative of specific cerebral behavior patterns in patients with PD.

This study has several limitations, including the fact that our evaluation was focused on overall long-term motor improvement, and we did not assess issues such as posture, gait, and articulation disturbances following long-term stimulation [46, 47]. It is also restricted by its retrospective, single-center design, meaning we only have MRI from our center. This limitation makes it difficult for us to validate our findings across multiple centers or use different types of scanning devices. Additionally, conducting repeated scans on patients using the same device to confirm the stability of the results is also challenging due to the retrospective nature of this study. Finally, due to limitations in sample size, we were unable to conduct comparisons between subtypes, and the grouping method employed was somewhat broad to enhance statistical sensitivity.

CONCLUSIONS

In conclusion, our findings suggest a potential correlation between individual structural covariance network fingerprints in PD patients and long-term motor outcomes following STN-DBS. However, it is important to interpret these results cautiously, as further validation and larger-scale multi-center studies are needed to confirm the robustness and generalizability of this observed association. The integrity of network topology, along with disruptions in network separations, is closely intertwined with long-term motor prognosis. Furthermore, we have identified that continuous and binary structural covariation network connections between the cerebellum, basal ganglia, frontal cortex and PCL can predict the motor improvement associated with STN-DBS at the individual patient level. The weighted T1 measure,

apart from serving as a necessary tool for preoperative localization, holds promise as a valuable biomarker for preoperative assessment of DBS candidates based on their individual structural covariation network fingerprints.

ACKNOWLEDGMENTS

This project was supported by National Natural Science Foundation of China (81830033, 81671104, 61761166004).

REFERENCES

1. Mosley PE, Paliwal S, Robinson K, et al. The structural connectivity of subthalamic deep brain stimulation correlates with impulsivity in Parkinson's disease. *Brain*. 2020;143(7):2235-54.

2. Hacker ML, Turchan M, Heusinkveld LE, et al. Deep brain stimulation in early-stage Parkinson disease: Five-year outcomes. *Neurology*. 2020;95(4):e393-e401.

3. Cavallieri F, Fraix V, Bove F, et al. Predictors of Long-Term Outcome of Subthalamic Stimulation in Parkinson Disease. *Ann Neurol*. 2021;89(3):587-97.

4. Barbosa R, Guedes LC, Cattoni MB, et al. Long-term follow-up of subthalamic nucleus deep brain stimulation in patients with Parkinson's disease: An analysis of survival and disability milestones. *Parkinsonism Relat Disord*. 2023;118:105921.

5. Shin HW, Kim MS, Kim SR, et al. Long-term Effects of Bilateral Subthalamic Deep Brain Stimulation on Postural Instability and Gait Difficulty in Patients with Parkinson's Disease. *J Mov Disord*. 2020;13(2):127-32.

6. Rodriguez-Oroz MC, Moro E, Krack P. Long-term outcomes of surgical therapies for Parkinson's disease. *Mov Disord*. 2012;27(14):1718-28.

7. Wolke R, Becktepe JS, Paschen S, et al. The Role of Levodopa Challenge in Predicting the Outcome of Subthalamic Deep Brain Stimulation. *Mov Disord Clin Pract*. 2023;10(8):1181-91.

8. Zheng Z, Yin Z, Zhang B, et al. Levodopa Challenge Test Predicts STN-DBS Outcomes in Various Parkinson's Disease Motor Subtypes: A More Accurate Judgment. *Neural Plast*. 2021;2021:4762027.

9. Piboolnurak P, Lang AE, Lozano AM, et al. Levodopa response in long-term bilateral subthalamic stimulation for Parkinson's disease. *Mov Disord*. 2007;22(7):990-7.

10. Lin W, Shi D, Wang D, et al. Can Levodopa Challenge Testing Predict the Effect of Deep Brain Stimulation? One-Year Outcomes in a Chinese Cohort. *Front Aging Neurosci*. 2021;13:764308.

11. Geraedts VJ, van Vugt JPP, Marinus J, et al. Predicting Motor Outcome and Quality of Life After Subthalamic Deep Brain Stimulation for Parkinson's Disease: The Role of Standard Screening Measures and Wearable-Data. *J Parkinsons Dis*. 2023;13(4):575-88.

12. Chu C, He N, Zeljic K, et al. Subthalamic and pallidal stimulation in Parkinson's disease induce distinct brain topological reconstruction. *Neuroimage*. 2022;255:119196.

13. Feigin A, Kaplitt MG, Tang C, et al. Modulation of metabolic brain networks after subthalamic gene therapy for Parkinson's disease. *Proc Natl Acad Sci U S A*. 2007;104(49):19559-64.

14. Logothetis NK. What we can do and what we cannot do with fMRI. *Nature*. 2008;453(7197):869-78.

15. Horn A, Reich M, Vorwerk J, et al. Connectivity Predicts deep brain stimulation outcome in Parkinson disease. *Ann Neurol*. 2017;82(1):67-78.

16. Yang B, Wang X, Mo J, et al. The altered spontaneous neural activity in patients with Parkinson's disease and its predictive value for the motor improvement of deep brain stimulation. *Neuroimage Clin*. 2023;38:103430.

17. Elliott ML, Knodt AR, Hariri AR. Striving toward translation: strategies for reliable fMRI measurement. *Trends Cogn Sci*. 2021;25(9):776-87.

18. Yin Z, Bai Y, Zou L, et al. Balance response to levodopa predicts balance improvement after bilateral subthalamic nucleus deep brain stimulation in Parkinson's disease. *NPJ Parkinsons Dis*. 2021;7(1):47.

19. Gracien RM, Maiworm M, Bruche N, et al. How stable is quantitative MRI? - Assessment of intra- and inter-scanner-model reproducibility using identical acquisition sequences and data analysis programs. *Neuroimage*. 2020;207:116364.

20. Liu Z, Palaniyappan L, Wu X, et al. Resolving heterogeneity in schizophrenia through a novel systems approach to brain structure: individualized structural covariance network analysis. *Molecular Psychiatry*. 2021;26(12):7719-31.

21. Lu L, Xu K, Shi L, et al. Measuring Subthalamic Nucleus Volume of Parkinson's Patients and Evaluating Its Relationship with Clinical Scales at Pre- and Postdeep Brain Stimulation Treatment: A Magnetic Resonance Imaging Study. *Biomed Res Int*. 2021;2021:6646416.

22. Muthuraman M, Deuschl G, Koirala N, et al. Effects of DBS in parkinsonian patients depend on the structural integrity of frontal cortex. *Sci Rep*. 2017;7:43571.

23. Chen Y, Zhu G, Liu Y, et al. Predict initial subthalamic nucleus stimulation outcome in Parkinson's disease with brain morphology. *CNS Neurosci Ther*. 2022;28(5):667-76.

24. Ping L, Sun S, Zhou C, et al. Altered topology of individual brain structural covariance networks in major depressive disorder. *Psychol Med*. 2023:1-12.

25. Li R, Zou T, Wang X, et al. Basal ganglia atrophy-associated causal structural network degeneration in Parkinson's disease. *Hum Brain Mapp*. 2022;43(3):1145-56.

26. Hughes AJ, Daniel SE, Kilford L, et al. Accuracy of clinical diagnosis of idiopathic Parkinson's disease: a clinico-pathological study of 100 cases. *J Neurol Neurosurg Psychiatry*. 1992;55(3):181-4.

27. Jost ST, Kaldenbach MA, Antonini A, et al. Levodopa Dose Equivalency in Parkinson's Disease: Updated Systematic Review and Proposals. *Mov Disord*. 2023;38(7):1236-52.

28. Goetz CG, Tilley BC, Shaftman SR, et al. Movement Disorder Society-sponsored revision of the Unified Parkinson's Disease Rating Scale (MDS-UPDRS): scale presentation and clinimetric testing results. *Mov Disord*. 2008;23(15):2129-70.

29. Schrag A, Sampaio C, Counsell N, et al. Minimal clinically important change on the unified Parkinson's disease rating scale. *Mov Disord*. 2006;21(8):1200-7.

30. Liu X, Wang Y, Ji H, et al. Personalized characterization of diseases using sample-specific networks. *Nucleic Acids Res*. 2016;44(22):e164.

31. Jenkinson M, Bannister P, Brady M, et al. Improved optimization for the robust and accurate linear registration and motion correction of brain images. *Neuroimage*. 2002;17(2):825-41.

32. Pedregosa F, Varoquaux G, Gramfort A, et al. Scikit-learn: Machine learning in Python. *the Journal of machine Learning research*. 2011;12:2825-30.

33. Zaidel A, Bergman H, Ritov Y, et al. Levodopa and subthalamic deep brain stimulation responses are not congruent. *Mov Disord*. 2010;25(14):2379-86.

34. Dembek TA, Roediger J, Horn A, et al. Probabilistic sweet spots predict motor outcome for deep brain stimulation in Parkinson disease. *Ann Neurol*. 2019;86(4):527-38.

35. Fasano A, Romito LM, Daniele A, et al. Motor and cognitive outcome in patients with Parkinson's disease 8 years after subthalamic implants. *Brain*. 2010;133(9):2664-76.

36. Lozano AM, Lipsman N, Bergman H, et al. Deep brain stimulation: current challenges and future directions. *Nat Rev Neurol*. 2019;15(3):148-60.

37. Shang S, Zhang H, Feng Y, et al. Region-Specific Neurovascular Decoupling Associated With Cognitive Decline in Parkinson's Disease. *Front Aging Neurosci*. 2021;13:770528.

38. Deng X, Liu Z, Kang Q, et al. Cortical Structural Connectivity Alterations and Potential Pathogenesis in Mid-Stage Sporadic Parkinson's Disease. *Front Aging Neurosci*. 2021;13:650371.

39. Yan S, Lu J, Li Y, et al. Impaired topological properties of cortical morphological brain networks correlate with motor symptoms in Parkinson's disease. *J Neuroradiol*. 2023.

40. Hacker ML, Rajamani N, Neudorfer C, et al. Connectivity Profile for Subthalamic Nucleus Deep Brain Stimulation in Early Stage Parkinson Disease. *Ann Neurol*. 2023;94(2):271-84.

41. David FJ, Goelz LC, Tangonan RZ, et al. Bilateral deep brain stimulation of the subthalamic nucleus increases pointing error during memory-guided sequential reaching. *Exp Brain Res*. 2018;236(4):1053-65.

42. Neumann WJ, Schroll H, de Almeida Marcelino AL, et al. Functional segregation of basal ganglia pathways in Parkinson's disease. *Brain*. 2018;141(9):2655-69.

43. Irmady K, Hale CR, Qadri R, et al. Blood transcriptomic signatures associated with molecular changes in the brain and clinical outcomes in Parkinson's disease. *Nat Commun*. 2023;14(1):3956.

44. Castrioto A, Lozano AM, Poon YY, et al. Ten-year outcome of subthalamic stimulation in Parkinson disease: a blinded evaluation. *Arch Neurol*. 2011;68(12):1550-6.

45. Rabel C, Le Goff F, Lefaucheur R, et al. Subjective Perceived Motor Improvement after Acute Levodopa Challenge in Parkinson's Disease. *J Parkinsons Dis*. 2016;6(4):779-85.

46. Jahanshahi M, Leimbach F, Rawji V. Short and Long-Term Cognitive Effects of Subthalamic Deep Brain Stimulation in Parkinson's Disease and Identification of Relevant Factors. *J Parkinsons Dis*. 2022;12(7):2191-209.

47. Guimaraes TG, Cury RG. Troubleshooting Gait Problems in Parkinson's Disease Patients with Subthalamic Nucleus Deep Brain Stimulation. *J Parkinsons Dis*. 2022;12(2):737-41.

48. Fan SY, Wang KL, Hu W, et al. Pallidal versus subthalamic nucleus deep brain stimulation for levodopa-induced dyskinesia. *Ann Clin Transl Neurol*. 2020;7(1):59-68.

49. Rolls ET, Huang CC, Lin CP, et al. Automated anatomical labelling atlas 3. *Neuroimage*. 2020;206:116189.

Table 1: Baseline and Follow-up

	Preoperate Mean±SD (range)	Postoperate Mean±SD (range)	*p*
Sex (M/F)	73/65	73/65	-
Age (years)	62.08±8.52 (35-82)	62.08±8.52 (35-82)	-
Durations (years)	11.72±4.73 (5-29)	11.72±4.73 (5-29)	-
LEDD (mg)	773.37±351.27 (0-1735.65)	555.66±291.21 (0-1580)	<0.001
MDS-UPDRS-III (med off)	49.86±16.00 (18-97)	24.61±13.49 (3-65)	<0.001
MDS-UPDRS-III-tremor (med off)	10.95±7.68 (0-33)	3.33±4.35 (0-22)	<0.001
MDS-UPDRS-III-rigidity (med off)	8.78±3.67 (2-23)	2.75±2.92 (0-12)	<0.001
FOGQ	11.58±8.22 (0-24)	7.54±7.47 (0-24)	<0.001
Berg	37.62±13.36 (1-56)	45.84±10.21 (2-56)	<0.001
MoCA	21.82±4.22 (10-30)	21.90±4.39 (10-30)	0.564
HAMA	18.41±9.53 (2-51)	12.31±8.57 (0-44)	<0.001
HAMD	18.25±9.18 (1-58)	13.85±10.15 (0-55)	<0.001

Outcome changes from baseline to follow-up of each group were tested using Wilcoxon signed-rank tests. MDS-UPDRS: Movement Disorder Society-sponsored Unified Parkinson's Disease Rating Scale; Berg: Berg balance scale; FOG-Q: freezing of gait questionnaire; MoCA: cognitive assessments using the Montreal cognitive assessment; HAMA: Hamilton Anxiety Rating Scale; HAMD: Hamilton Depression Rating Scale.

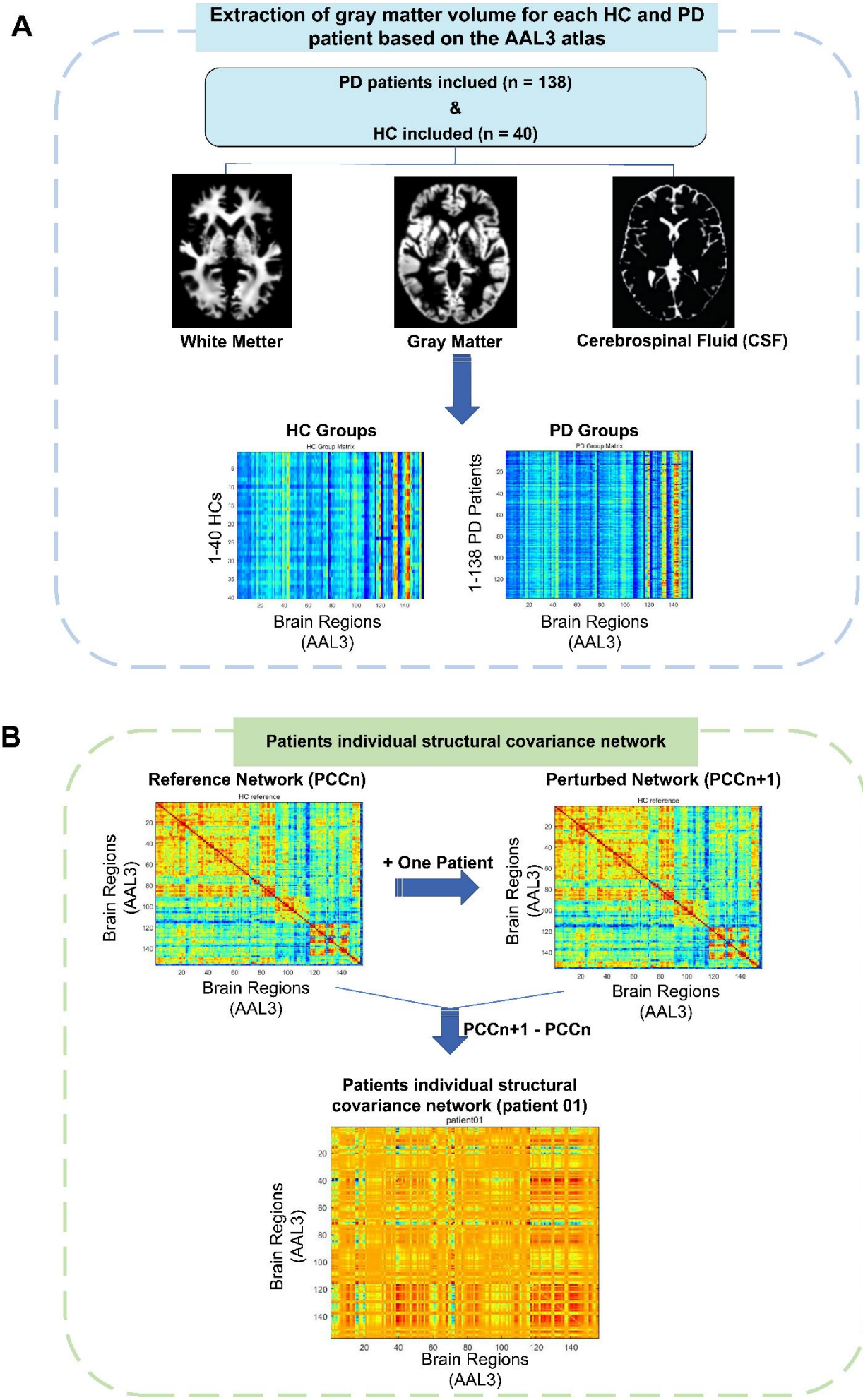
A
Extraction of gray matter volume for each HC and PD patient based on the AAL3 atlas
PD patients inclued (n = 138)
&
HC included (n = 40)
White Metter
Gray Matter
Cerebrospinal Fluid (CSF)
HC Groups
PD Groups
HC Group Matrix
PD Group Matrix
1-40 HCs
1-138 PD Patients
Brain Regions (AAL3)
Brain Regions (AAL3)
B
Patients individual structural covariance network
Reference Network (PCCn)
Perturbed Network (PCCn+1)
HC reference
HC reference
+ One Patient
Brain Regions (AAL3)
Brain Regions (AAL3)
Brain Regions (AAL3)
Brain Regions (AAL3)
PCCn+1 - PCCn
Patients individual structural covariance network (patient 01)
patient01
Brain Regions (AAL3)
Brain Regions (AAL3)

Figure 1: Schematic outline of the study. A: Gray matter volumes were computed using the CAT12 toolbox, and gray matter volumes were extracted based on the AAL3 atlas for all HC and PD patients. B: Individual structural covariance network computation process for patients. PCC: Pearson correlation coefficient; HC: Health Controls; PD: Parkinson's disease.

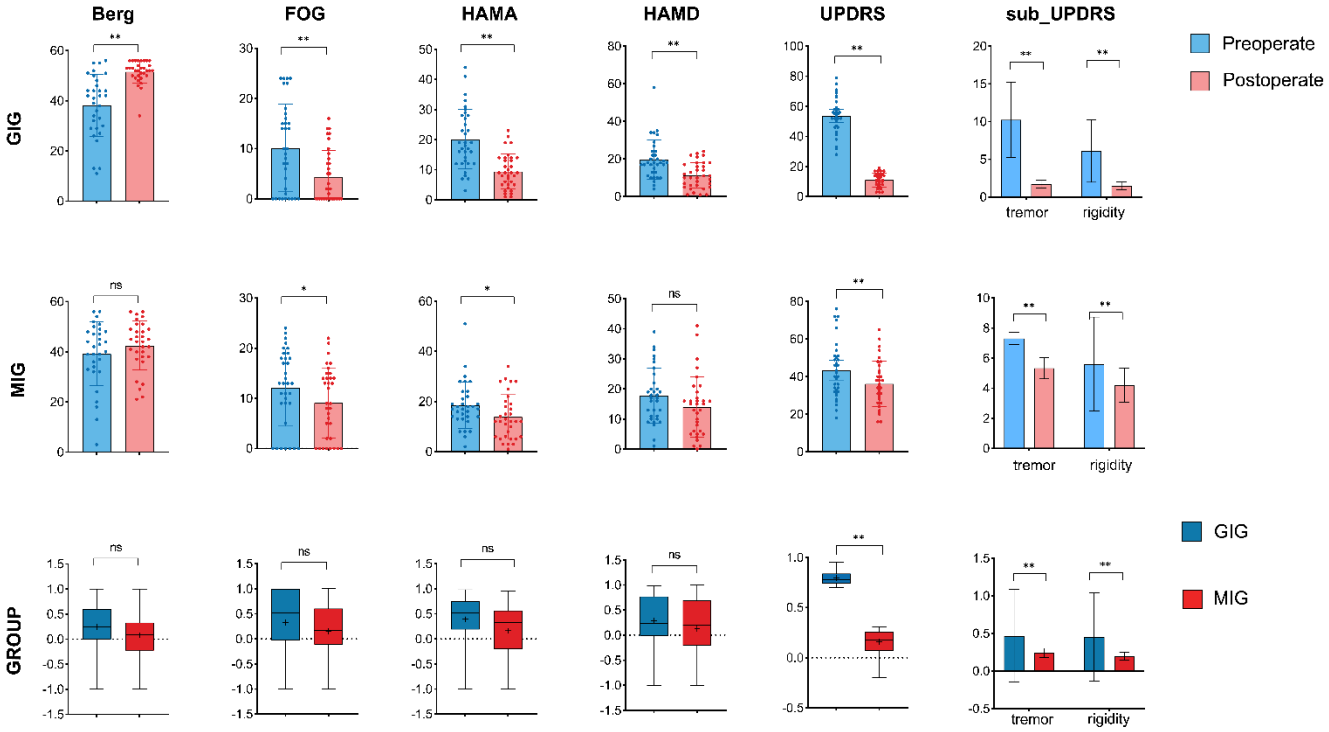

Figure 2: Clinical Improvement: A, B: Differences in preoperative and long-term postoperative scores for motor and non-motor scales in patients with DBS improvement rates in the GIG (A) and MIG (B). Paired t-tests were conducted for data passed the normality test, while the Wilcoxon signed-rank test was used for data did not meet the normality assumption. C: Comparison of the improvement rates in motor and non-motor symptoms between the GIG and MIG. For normally distributed data, a two-sample t-test was employed, whereas the Wilcoxon rank-sum test was used for data that did not meet the normality assumption. GIG: good improvement group; MIG: moderate improvement group.

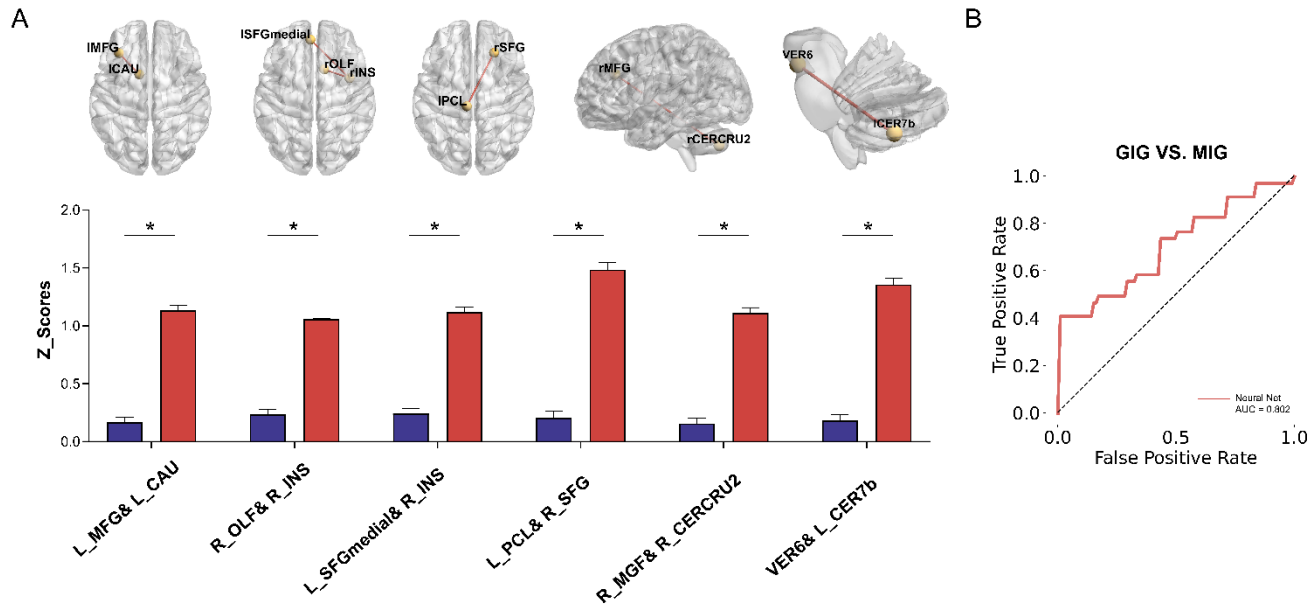

Figure 3: Inter-group Differences in Edges and Prediction: A Comparison of inter-group differences in edges between the GIG (blue) and MIG (red) patient groups for edges that are correlated with DBS improvement rate and ranked in the top 1%. Age, gender, TIV, and MoCA were included as covariates. FDR correction, significant inter-group differences are found in all six edges. B: Prediction of Long-Term Improvement Groups in Patients Using 6 Edge Features. TIV: Total Intracranial Volume; MoCA: Montreal Cognitive Assessment; FDR: Following False Discovery Rate; GIG: good improvement group; MIG: moderate improvement group.

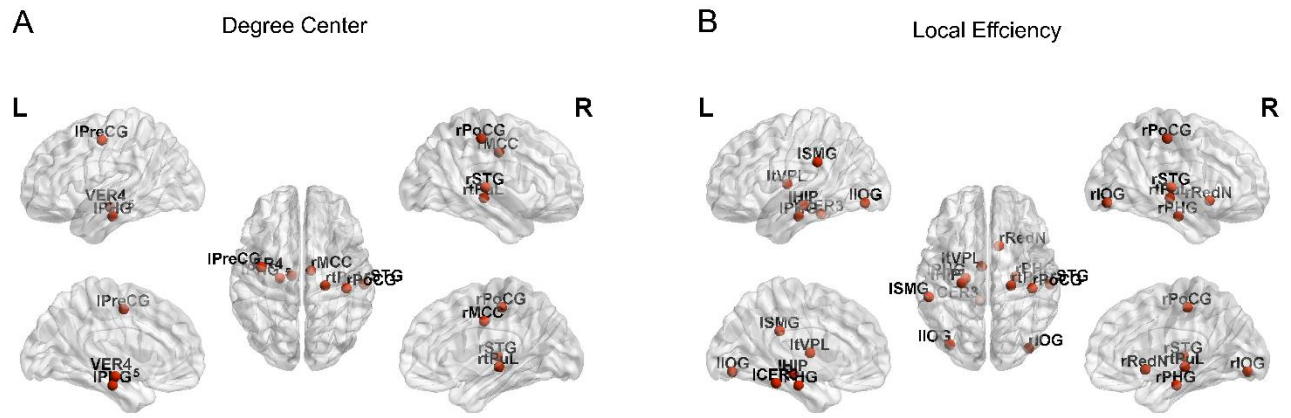

Figure 4: The Relationship Between Graph Theory Metrics and Long-Term Treatment Outcomes. Red spherical nodes represent brain regions with P-values corrected for false discovery rate (FDR) below 0.05. A: Degree centrality of nodes that correlated with long-term motor prognosis. B: Local efficiency of nodes that correlated with long-term motor prognosis.

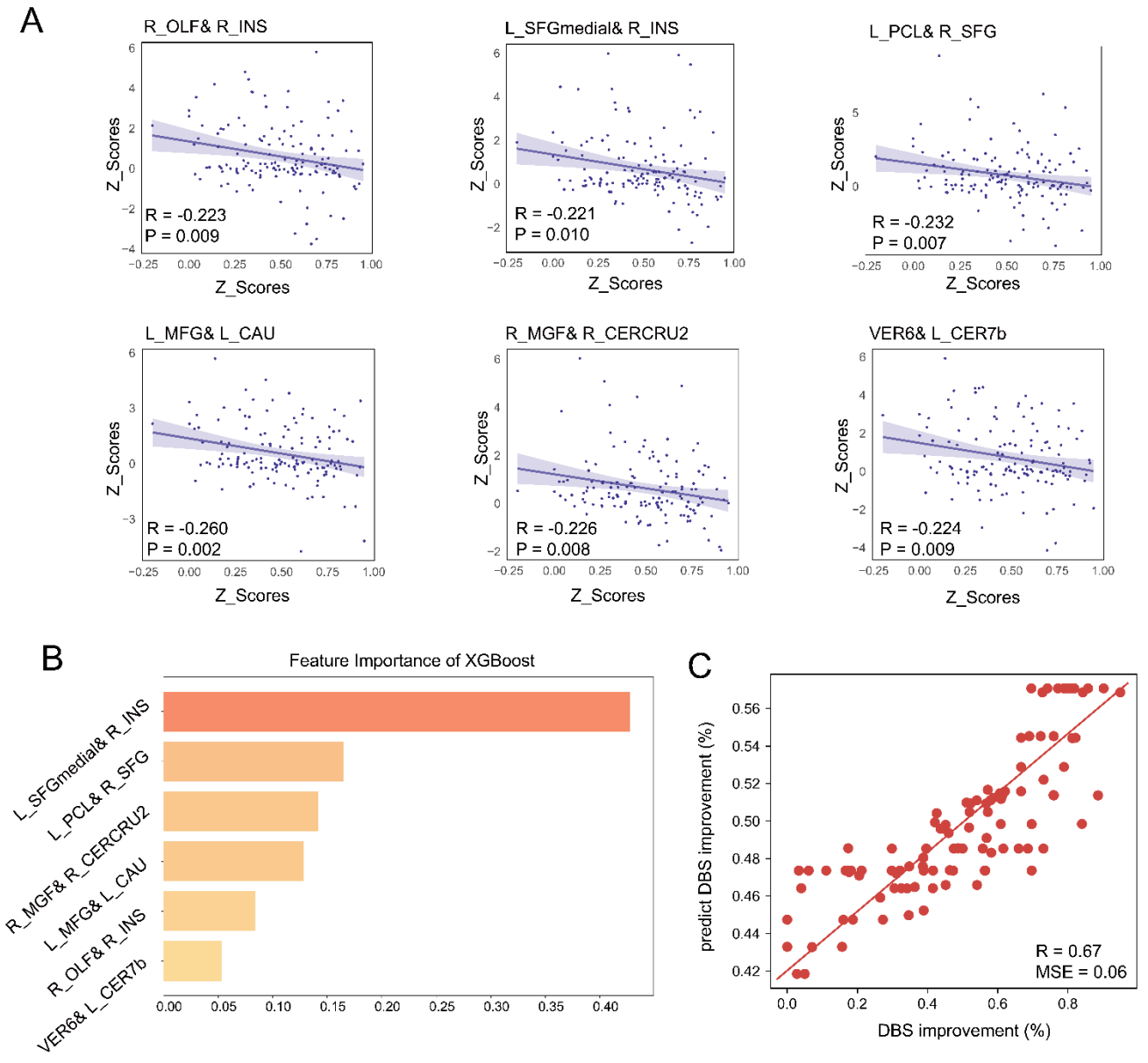

Figure 5: Individual Structural Covariance Networks for Predicting Long-Term Treatment Outcomes. A: six edges of correlations with DBS improvement rates, with age, gender, and TIV as covariates. B: Weights of the six edges in predicting long-term DBS improvement rates using the XGBoost model. C: Correlation between the actual and predicted values of long-term DBS improvement rates for the six edges using the XGBoost model.

SUPPLEMENTAL FILES

STN-DBS surgery and follow-up protocol

The standard procedure for DBS was performed as previously reported [48]. All patients received bilateral electrode implantation into the STN using either model 3389 electrodes (Medtronic, USA) or model L301 electrodes (Pins Medical, China). In brief, electrode implantation was conducted under local anesthesia with the guidance of a Leksell micro-stereotactic system (Elekta Instrument AB, Stockholm, Sweden). Intraoperative microelectrode recording and macro-stimulation tests were conducted for trajectory selection. Subsequently, an implantable pulse generator (IPG) connected to the electrodes was implanted in the subclavicular area under general anesthesia. Electrode placement was confirmed through CT scanning or lead reconstruction.

At follow-up stage, patients returned to the hospital for programming to adjust stimulation parameters based on clinical symptoms. Following a 3-7 days observation period (depending on the patient's schedule), patients were then referred to the assessment center for evaluations. Med-OFF assessments were conducted after at least 12 hours of medication withdrawal, and Med-ON assessments were performed approximately 1 hour after medication intake. All assessments were recorded with the consent of the patients.

T1 data acquisition and preprocessing

All participants underwent scanning using a 3T MRI system (Siemens Medical Systems) equipped with a 32-channel head coil. Head immobilization was achieved using head cushions to ensure accuracy during imaging. A whole-head three-dimensional sagittal T1-weighted 3D magnetization-prepared rapid acquisition gradient echo (MPRAGE) sequence was employed with the following parameters: repetition time, 1.56 ms; echo time, 0.00169 ms; flip angle, 8°; matrix size, 256 × 256; isotropic voxel size, 1 × 1 × 1 mm^3; and 196 slices were acquired.

T1-weighted structural data were subjected to voxel-based morphometric preprocessing using CAT12 (http://dbm.neuro.unijena.de/cat). The preprocessing steps closely followed those outlined in Liu's study [20] which included: (1) the T1-weighted images underwent segmentation into GM, white matter (WM), and non-brain voxels (cerebrospinal fluid, skull) using the "new-segment" routine. (2) Population templates for GM and WM were generated from each dataset using the DARTEL algorithm. (3) The gray-matter images were aligned to a nonlinear deformation field and normalized to MNI space. (4) extraction of gray matter volumes based on the AAL3 atlas. Data quality checks using CAT12, we ensured that data from 138 patients and 40 HC all met the criterion of a weighted average (interquartile range, IQR) above 75%. Additionally, a check of the data confirmed its overall integrity and absence of anomalies. Due to the low variance of voxels with low gray matter values, rendering them unsuitable for Gaussian error distribution, we applied a masking procedure using the SPM toolbox (http://www0.cs.ucl.ac.uk/staff/g.ridgway/masking/) and set the threshold at 0.2 [20].

The AAL3 atlas divided the brain into 170 regions of interest (85 in each hemisphere) for identifying brain regions [49]. Brain regions composed of voxels with excessively low gray matter volumes were excluded. Ultimately, 156 brain regions were included in the study, and the specific regions included are detailed in Table S4.

Definition of Graph Theory Metrics

Small-World Attributes: A network is considered a small-world network when it exhibits high clustering (like regular networks) and short average path lengths (like random networks). This combination allows for efficient local and global information transfer.

Global Efficiency: Global efficiency measures how well information is exchanged across the entire network. It is calculated as the average inverse shortest path length between all pairs of nodes in the network.

Degree Centrality: Degree centrality of a node is the number of edges connected to that node. Nodes with higher degree centrality are more central to the network structure and are often considered more influential.

Local Efficiency: Local efficiency measures the efficiency of information exchange within the immediate neighborhood of a node. It is defined as the inverse of the shortest path length (number of steps, or links, between network nodes) between connected nodes that are neighbors with the node of interest.

Table S1. Long-Term Follow-Up Improvement Percentage in GIG and MIG

	GIG	MIG	HC	*P*
Gender (M/F)	16/18	15/19	21/19	0.768
Age (years)	60.29±8.19	62.21±7.75	60.83±6.14	0.327
Durations (years)	11.32±3.74	12.18±5.41		0.452
Levodopa Responsiveness	0.56±0.23	0.56±0.19		0.854[b]
MDS-UPDRS-III	0.79±0.07	0.16±0.11		<0.001
MDS-UPDRS-III-tremor	0.85±0.27	0.29±0.71		0.001
MDS-UPDRS-III-rigidity	0.87±0.20	0.34±0.46		<0.001
FOGQ	0.33±0.76	0.15±0.62		0.107
Berg	0.24±0.49	0.07±0.49		0.082
MoCA	0.06±0.27	-0.02±0.45		0.803
HAMA	0.39±0.49	0.16±0.58		0.085
HAMD	0.29±0.47	0.13±0.63		0.390

Age and gender among three groups using a one-way analysis of variance (ANOVA). All results are presented as mean ± standard deviation. Comparisons between the GIG and MIG groups were subjected to a normality test, and for data following a normal distribution, a two-sample t-test (denoted as 'b') was employed. Non-normally distributed data were analyzed using Mann-Whitney U-tests. GIG: good improvement group; MIG: moderate improvement group; HC: health controls; MDS-UPDRS: Movement Disorder Society-sponsored Unified Parkinson's Disease Rating Scale; Berg: Berg balance scale; FOG-Q: freezing of gait questionnaire; MoCA: cognitive assessments using the Montreal cognitive assessment; HAMA: Hamilton Anxiety Rating Scale; HAMD: Hamilton Depression Rating Scale.

Table S2. Programming parameters between groups

	MIG		GIG		
	L	R	L	R	P
Voltage	2.57±0.56	2.56±0.56	2.51±0.63	2.55±0.58	0.605
Frequency	135.79±24.06		134.71±24.64		0.868[b]
Pulse Width	75.59±11.33	77.06±14.04	74.41±13.30	75.29±13.31	0.578

The frequencies for the two patient groups were compared using the Mann-Whitney U test, and the results were denoted as "b." Voltage and pulse width were analyzed using one-way ANOVA to assess whether there were any differences between the left and right sides for both groups of patients. All results are presented as mean ± standard deviation. GIG: good improvement group; MIG: moderate improvement group; L: left limbs; R: right limbs.

Table S3. The programming of every patient

Group	L				R				
		PW	F	Vol		PW	F	Vol	
MIG	C+2-	80	185	3.2	C+9-	130	185	3.5	Medtronic
MIG	C+1-	80	137	2.7	C+7-	70	137	2.55	Pins
MIG	C+1-	60	135	1	C+10-	70	135	1.6	Medtronic
MIG	C+2-	90	100	3.5	C+9-11-	100	100	3.5	Medtronic
MIG	1+3-	70	125	1.95	C+7-	90	125	2.6	Pins
MIG	C+2-	70	140	3.05	C+11-	60	140	1.85	Medtronic
MIG	C+3-	80	80	3	C+6-	70	80	3	Pins
MIG	C+1-	90	100	2.85	C+9-	80	100	2.55	Medtronic
MIG	C+4-	60	160	2.6	C+8-	60	160	3	Pins
MIG	C+3-	80	155	2.5	C+8-	60	155	1.9	Pins
MIG	C+3-	70	135	2.7	C+7-	70	135	2.95	Pins
MIG	C+2-	60	135	1.9	C+6-	60	135	1.9	Pins
MIG	C+2-	60	140	2.7	C+6-	60	140	2.7	Pins
MIG	4+1-	80	150	3	C+5-	70	150	2.6	Pins
MIG	C+2-	70	145	3	C+10-	80	145	3	Medtronic
MIG	C+3-	100	155	2.75	C+7-	80	155	2.4	Pins
MIG	C+1-2-	80	100	3.6	C+6-8-	80	100	3.9	Pins
MIG	C+2-	90	150	2.5	C+10-	90	150	2.5	Medtronic
MIG	C+2-	60	130	2.3	C+10-	70	130	1.5	Medtronic
MIG	0+1-	80	140	2.7	0+9-	70	140	2.8	Medtronic
MIG	C+3-	90	135	3	C+6-	80	135	2.9	Pins
MIG	C+1-	80	160	2.45	C+9-	70	160	1.95	Medtronic
MIG	C+2-3-	90	165	3.15	C+6-7-	80	165	3.1	Pins
MIG	C+3-	70	150	2.3	C+10-	80	150	2.3	Medtronic
MIG	C+1-	90	90	2.7	C+10-	70	90	1.7	Medtronic
MIG	C+3-	70	90	2.3	C+11-	70	90	2.3	Medtronic
MIG	C+2-	90	140	3	C+10-	80	140	2.6	Medtronic
MIG	C+3-	60	160	1.5	C+7-	90	160	2.8	Pins

MIG	C+1-	70	120	2.4	C+9-	90	120	3.3	Medtronic
MIG	C+4-	60	130	3	C+8-	60	130	2	Pins
MIG	C+3-	70	160	2	8+10-	90	160	2.5	Medtronic
MIG	C+3-	70	145	2.15	C+8-	80	145	2.6	Pins
MIG	C+2-	70	125	1.8	C+6-	80	125	2.5	Pins
MIG	C+2-	80	150	2	C+8-	80	150	2.3	Pins
EIG	C+2-	60	140	2.1	C+6-	60	140	2	Pins
EIG	C+3-	80	160	2.65	C+6-7-	60	160	3.3	Pins
EIG	C+2-	80	145	2.5	C+10-	80	145	2.3	Medtronic
EIG	C+2-	80	163	2.7	C+7-	90	163	2.85	Pins
EIG	C+1-3-	70	80	2.65	C+9-11-	70	80	2.65	Medtronic
EIG	C+2-	2.1	70	130	C+6-	2.15	70	130	Pins
EIG	C+3-	70	135	2.8	C+7-	70	135	2.8	Pins
EIG	C+2-	60	110	1.9	C+10-	60	110	1.9	Medtronic
EIG	0+3-	70	140	1.7	0+9-	70	140	2.3	Medtronic
EIG	C+1-	110	90	3.2	C+9-	100	90	3.5	Medtronic
EIG	C+3-	60	140	2	C+7-	70	140	2.7	Pins
EIG	C+2-	70	90	2.9	C+10-	80	90	2.9	Medtronic
EIG	c+1-3-	80	155	2.4	C+11-	80	155	2.5	Medtronic
EIG	C+3-4-	60	130	1.5	C+8-	90	130	2.4	Pins
EIG	C+4-	60	130	1.55	C+8-	60	130	1.55	Pins
EIG	C+1-	100	95	3.15	C+10-	100	95	3.25	Medtronic
EIG	C+3-	60	160	2.4	C+7-	70	160	2.7	Pins
EIG	C+4-	100	160	3.5	C+7-	100	160	2.9	Pins
EIG	0+2-	70	150	2.2	0+10-	60	150	2.15	Medtronic
EIG	C+1-	90	145	3.05	C+9-	80	145	1.8	Medtronic
EIG	C+2-3-	90	153	3.2	C+7-6-	90	153	3.2	Pins
EIG	C+1-	70	70	2.5	C+5-	70	70	2.6	Pins
EIG	C+2-	70	135	2.2	C+10-	70	135	1.9	Medtronic
EIG	C+3-	70	140	2.45	C+6-	70	140	2.45	Pins
EIG	C+3-	90	127	3.75	C+7-	80	127	3.75	Pins
EIG	C+3-	70	155	2.3	C+10-	100	155	2.8	Medtronic
EIG	C+1-	80	160	2.85	C+9-	80	160	2.75	Medtronic
EIG	C+3-	70	160	3.3	C+7-	60	160	2.3	Pins
EIG	C+2-	70	130	2.3	C+10-	60	130	1.7	Medtronic
EIG	C+3-	90	127	3.75	C+7-	80	127	3.75	Pins
EIG	C+2-	60	135	1.4	C+10-	60	135	1.8	Medtronic
EIG	C+2-	60	145	1.6	C+10-	70	145	2.2	Medtronic
EIG	C+2-	60	135	2	C+10-	60	135	2.1	Medtronic
EIG	C+2-	80	160	2.95	C+9-10-	90	160	3	Medtronic

The provided information details the programmable contact points and parameters for two groups of patients. The final column contains manufacturer-specific data, as different manufacturers have varying configurations for these contact points. In the case of "Pins", the contact points are sequentially assigned as follows: left limbs (1-2-3-4) and right limbs (5-6-7-8). In contrast, for "Medtronic", the contact points are sequentially assigned as follows: left limbs (0-1-2-3) and right limbs (8-9-10-11). "C+" denotes stimulation of the overall circulatory system.

Table S4. After excluding brain regions with predominantly zero gray matter volume, the remaining brain regions and their coordinates within the AAL3 atlas.

Label	Number		
'Precentral_L'	1	1	[-38.4302325581395,-7.46142938173568,49.1403857061826]

'Precentral_R'	2	2	[41.6008577343981,-10.0498373262348,50.3098195800059]
'Frontal_Sup_2_L'	3	3	[-19.6679671457906,35.4552361396304,34.7373716632443]
'Frontal_Sup_2_R'	4	4	[23.0513070620367,32.6927428794382,36.8437378072571]
'Frontal_Mid_2_L'	5	5	[-35.0269580652319,32.3728644331041,29.4378744175727]
'Frontal_Mid_2_R'	6	6	[39.2736625514403,32.3823045267490,28.8164609053498]
'Frontal_Inf_Oper_L'	7	7	[-48.2957610789981,10.9913294797688,17.3015414258189]
'Frontal_Inf_Oper_R'	8	8	[50.4270907791280,13.1754824874911,19.6958541815583]
'Frontal_Inf_Tri_L'	9	9	[-45.3900751285093,28.1666666666667,12.0828390668248]
'Frontal_Inf_Tri_R'	10	10	[50.5613668061367,28.4019060901906,12.3172942817294]
'Frontal_Inf_Orb_2_L'	11	11	[-40.8734643734644,30.5565110565111,-8.57616707616708]
'Frontal_Inf_Orb_2_R'	12	12	[46.3260869565218,32.9187643020595,-8.48855835240275]
'Rolandic_Oper_L'	13	13	[-46.8785425101215,-10.2510121457490,12.1356275303644]
'Rolandic_Oper_R'	14	14	[52.8816679188580,-8.03719008264463,12.8298271975958]
'Supp_Motor_Area_L'	15	15	[-5.19073125291104,3.05006986492779,59.5642757335818]
'Supp_Motor_Area_R'	16	16	[8.74630957401941,-1.59320961619569,60.0128637705610]
'Olfactory_L'	17	17	[-7.36831359738669,13.5063291139240,-12.6047366271948]
'Olfactory_R'	18	18	[10.6798072711345,14.1498028909330,-13.1686377573368]
'Frontal_Sup_Medial_L'	19	19	[-4.67379679144385,47.3870320855615,29.1363636363636]
'Frontal_Sup_Medial_R'	20	20	[9.25070290534208,49.0285848172446,28.4268978444236]
'Frontal_Med_Orb_L'	21	21	[-4.93810848400557,52.0173852573018,-9.35674547983310]
'Frontal_Med_Orb_R'	22	22	[8.33411214953271,49.9065420560748,-9.01635514018692]
'Rectus_L'	23	23	[-4.94131455399061,35.2065727699531,-20.0680751173709]
'Rectus_R'	24	24	[8.50268456375839,33.9510067114094,-19.9362416107383]
'OFCmed_L'	25	25	[-13.7363636363636,35.1181818181818,-21.5836363636364]
'OFCmed_R'	26	26	[16.9219001610306,36.5982286634461,-21.7592592592593]
'OFCant_L'	27	27	[-24.5383747178330,46.2629796839729,-16.6128668171558]
'OFCant_R'	28	28	[29.1018518518518,47.9629629629630,-16.6820987654321]
'OFCpost_L'	29	29	[-28.1631393298060,22.9003527336861,-19.9955908289242]
'OFCpost_R'	30	30	[33.5303030303030,24.3627450980392,-19.8868092691622]
'OFClat_L'	31	31	[-42.0279187817259,39.3578680203046,-15.6167512690355]
'OFClat_R'	32	32	[48.2553191489362,36.2234042553191,-16.7446808510638]
'Insula_L'	33	33	[-34.9101184068891,4.94025834230357,1.67222820236813]
'Insula_R'	34	34	[39.2220338983051,4.52033898305083,0.313559322033896]
'Cingulate_Ant_L'	35		[0,0,0]
'Cingulate_Ant_R'	36		[0,0,0]
'Cingulate_Mid_L'	37	35	[-5.38253477588872,-16.6009788768676,39.7143225141680]
'Cingulate_Mid_R'	38	36	[8.16409441670450,-10.6970040853382,37.9375851112120]
'Cingulate_Post_L'	39	37	[-4.70518358531318,-44.6727861771058,22.7786177105832]
'Cingulate_Post_R'	40	38	[7.67611940298508,-43.5865671641791,19.9716417910448]
'Hippocampus_L'	41	39	[-24.7553648068670,-22.4635193133047,-11.8841201716738]
'Hippocampus_R'	42	40	[29.4450317124736,-21.4915433403805,-12.0771670190275]
'ParaHippocampal_L'	43	41	[-20.9928425357873,-17.7924335378323,-22.4182004089980]
'ParaHippocampal_R'	44	42	[25.6484098939929,-16.8003533568905,-22.2438162544170]
'Amygdala_L'	45	43	[-23.0090909090909,-2.44545454545455,-18.9545454545455]
'Amygdala_R'	46	44	[27.5564516129032,-1.07258064516130,-19.3064516129032]
'Calcarine_L'	47	45	[-6.98272807794508,-80.3210806023029,4.60363153232950]
'Calcarine_R'	48	46	[16.2098334228909,-74.9492208490059,7.51934443847394]
'Cuneus_L'	49	47	[-5.76429980276134,-81.8622616699540,25.4040105193951]

'Cuneus_R'	50	48	[13.6896067415730,-81.0898876404494,26.3525280898876]
'Lingual_L'	51	49	[-14.3582338902148,-69.3649164677804,-6.50763723150358]
'Lingual_R'	52	50	[16.5773913043478,-68.6417391304348,-5.71565217391304]
'Occipital_Sup_L'	53	51	[-16.2569546120059,-86.1105417276720,26.3535871156662]
'Occipital_Sup_R'	54	52	[24.4631988676575,-82.7066525123850,28.7653927813164]
'Occipital_Mid_L'	55	53	[-32.1486983154671,-82.4877488514548,14.3024502297090]
'Occipital_Mid_R'	56	54	[37.6277407054338,-81.4933269780744,17.5676835081030]
'Occipital_Inf_L'	57	55	[-35.9824654622742,-80.0685441020191,-9.66471838469713]
'Occipital_Inf_R'	58	56	[38.3705763397371,-83.6911021233569,-9.49292214357937]
'Fusiform_L'	59	57	[-30.8893460372456,-41.8824166305760,-22.1093546990039]
'Fusiform_R'	60	58	[34.1592533756950,-40.6985702938840,-22.0337569499603]
'Postcentral_L'	61	59	[-42.4044193216855,-24.2754367934224,46.9568345323741]
'Postcentral_R'	62	60	[41.6582526811405,-27.2726916034528,50.7539890138635]
'Parietal_Sup_L'	63	61	[-23.2133171912833,-61.3077481840194,57.1571428571428]
'Parietal_Sup_R'	64	62	[26.3424842484248,-60.9284428442844,60.2137713771377]
'Parietal_Inf_L'	65	63	[-42.6066612178177,-47.5192071924806,44.9229668982428]
'Parietal_Inf_R'	66	64	[46.7914498141264,-48.0881040892193,47.6918215613383]
'SupraMarginal_L'	67	65	[-55.6464968152866,-35.4363057324841,28.6194267515924]
'SupraMarginal_R'	68	66	[57.7624113475177,-33.3176291793313,32.6347517730496]
'Angular_L'	69	67	[-43.9347826086957,-62.5818414322251,33.7830349531117]
'Angular_R'	70	68	[45.7283105022831,-61.7385844748858,36.8150684931507]
'Precuneus_L'	71	69	[-7.09070294784580,-57.8248299319728,46.1400226757370]
'Precuneus_R'	72	70	[10.1888208269525,-57.8139356814701,41.8607963246554]
'Paracentral_Lobule_L'	73	71	[-7.47479614529281,-27.1508524833210,68.1923647146034]
'Paracentral_Lobule_R'	74	72	[7.62679425837321,-33.4425837320574,66.2918660287081]
'Caudate_L'	75	73	[-12.1713430012610,8.56084489281210,10.6568411097100]
'Caudate_R'	76	74	[15.7480949589684,10.0067409144197,10.0822098475967]
'Putamen_L'	77	75	[-23.8852767666625,2.00476967490900,0.702146353709054]
'Putamen_R'	78	76	[28.0055300623603,3.16637251441347,0.707612660312975]
'Pallidum_L'	79	77	[-17.5614334470990,-1.85836177474403,-1.54436860068259]
'Pallidum_R'	80	78	[21.4214285714286,-1.55714285714286,-1.58571428571429]
'Thalamus_L'	81	79	[-41.8466666666667,-20.5355555555556,8.17555555555556]
'Thalamus_R'	82	80	[46.3795180722892,-18.6445783132530,8.54417670682732]
'Heschl_L'	83		[0,0,0]
'Heschl_R'	84		[0,0,0]
'Temporal_Sup_L'	85	81	[-52.9355400696864,-22.5095818815331,5.34059233449477]
'Temporal_Sup_R'	86	82	[58.3325374084687,-23.5105062082139,4.91865647882840]
'Temporal_Pole_Sup_L'	87	83	[-39.6540856031128,13.3677042801556,-21.9365758754864]
'Temporal_Pole_Sup_R'	88	84	[48.4372197309417,12.9573991031390,-18.6898355754858]
'Temporal_Mid_L'	89	85	[-55.3688789963578,-35.4842169162283,-4.08478348846622]
'Temporal_Mid_R'	90	86	[57.6599002041279,-39.0656611476525,-3.27523247902019]
'Temporal_Pole_Mid_L'	91	87	[-36.2443708609272,12.8006622516556,-35.8668874172185]
'Temporal_Pole_Mid_R'	92	88	[44.5404380791912,12.7468407750632,-34.0181128896377]
'Temporal_Inf_L'	93	89	[-49.5362500000000,-29.7918750000000,-25.0193750000000]
'Temporal_Inf_R'	94	90	[53.8820635366882,-32.6388810795614,-24.2306719145347]
'Cerebellum_Crus1_L'	95	91	[-34.8853246254322,-68.4431425278525,-30.7627737226277]
'Cerebellum_Crus1_R'	96	92	[38.7145015105740,-68.8716012084592,-31.3496978851964]
'Cerebellum_Crus2_L'	97	93	[-27.2687434002112,-75.0797254487856,-39.9435058078142]

'Cerebellum_Crus2_R'	98	94	[33.1735947094946,-70.8967879074162,-41.7017005196032]
'Cerebellum_3_L'	99	95	[-7.61764705882354,-38.8676470588235,-20.2794117647059]
'Cerebellum_3_R'	100	96	[13.5628019323672,-36.2101449275362,-21.0990338164251]
'Cerebellum_4_5_L'	101	97	[-13.8431111111111,-45.1631111111111,-18.7613333333333]
'Cerebellum_4_5_R'	102	98	[18.3885017421603,-44.6649245063879,-19.8542392566783]
'Cerebellum_6_L'	103	99	[-22.0253837072019,-60.7585596221960,-23.9805194805195]
'Cerebellum_6_R'	104	100	[25.9295264623955,-60.0376044568245,-25.4403899721449]
'Cerebellum_7b_L'	105	101	[-31.0897435897436,-61.5495726495727,-47.2521367521368]
'Cerebellum_7b_R'	106	102	[34.4288389513109,-64.9082397003745,-50.2602996254682]
'Cerebellum_8_L'	107	103	[-24.5291467938527,-56.2710651828299,-49.5545839957605]
'Cerebellum_8_R'	108	104	[26.2729636048527,-58.1308492201040,-51.2980935875217]
'Cerebellum_9_L'	109	105	[-9.75316455696202,-50.6887226697353,-47.7359033371692]
'Cerebellum_9_R'	110	106	[10.6903584672435,-51.2515451174289,-48.1242274412855]
'Cerebellum_10_L'	111	107	[-21.2916666666667,-35.5000000000000,-43.5694444444444]
'Cerebellum_10_R'	112	108	[27.3050314465409,-35.5188679245283,-43.1415094339623]
'Vermis_1_2'	113	109	[1.96402877697842,-40.6786570743405,-21.8705035971223]
'Vermis_3'	114	110	[2.55263157894737,-41.7894736842105,-13.2192982456140]
'Vermis_4_5'	115	111	[2.33458646616542,-54.0939849624060,-7.90150375939849]
'Vermis_6'	116	112	[2.26819407008087,-68.8504043126685,-16.8935309973046]
'Vermis_7'	117	113	[2.36597938144330,-73.6958762886598,-26.8505154639175]
'Vermis_8'	118	114	[2.31069958847736,-66.1543209876543,-35.8497942386831]
'Vermis_9'	119	115	[2.10919540229885,-56.6724137931034,-36.7988505747126]
'Vermis_10'	120	116	[1.64285714285714,-47.6250000000000,-33.3750000000000]
'Thal_AV_L'	121	117	[-5.94805194805196,-6.85714285714286,8.01948051948052]
'Thal_AV_R'	122	118	[5.34090909090909,-5.62500000000000,7.72159090909091]
'Thal_LP_L'	123	119	[-9.85922330097087,-16.9174757281553,14.7524271844660]
'Thal_LP_R'	124	120	[8.39062500000000,-14.7031250000000,14.0781250000000]
'Thal_VA_L'	125	121	[-10.7131537242472,-5.02218700475436,3.77812995245642]
'Thal_VA_R'	126	122	[10.3264000000000,-3.79840000000000,3.47040000000000]
'Thal_VL_L'	127	123	[-13.4018306636156,-12.2713958810069,6.84759725400458]
'Thal_VL_R'	128	124	[12.8835186080232,-11.0869985500242,6.45287578540358]
'Thal_VPL_L'	129	125	[-17.7706013363029,-21.4432071269488,5.34743875278396]
'Thal_VPL_R'	130	126	[16.8086560364465,-20.3940774487472,4.87547456340167]
'Thal_IL_L'	131	127	[-9.75476190476191,-18.0428571428571,-0.302380952380958]
'Thal_IL_R'	132	128	[9.37708830548927,-17.0525059665871,-0.369928400954649]
'Thal_Re_L'	133	129	[-5.50000000000000,-8.87500000000000,-4]
'Thal_Re_R'	134	130	[5.50000000000000,-9.12500000000000,-4.25000000000000]
'Thal_MDm_L'	135	131	[-4.75600000000000,-15.7140000000000,4.27800000000001]
'Thal_MDm_R'	136	132	[4.26181102362205,-15.1190944881890,3.77460629921259]
'Thal_MDl_L'	137	133	[-7.62837837837837,-14.6013513513514,5.06081081081081]
'Thal_MDl_R'	138	134	[7.20727272727272,-13.6690909090909,4.39636363636363]
'Thal_LGN_L'	139	135	[-22.6521739130435,-24.7420289855072,-5.61159420289854]
'Thal_LGN_R'	140	136	[21.7426273458445,-24.7828418230563,-5.02680965147454]
'Thal_MGN_L'	141	137	[-15.5735294117647,-24.9117647058823,-5.58088235294117]
'Thal_MGN_R'	142	138	[15.3333333333333,-24.4824561403509,-5.48245614035088]
'Thal_PuI_L'	143	139	[-17.6532258064516,-29.7540322580645,-0.294354838709680]
'Thal_PuI_R'	144	140	[16.7215686274510,-28.8745098039216,-0.501960784313724]
'Thal_PuM_L'	145	141	[-13.2900815217391,-28.2581521739130,6.37432065217391]

'Thal_PuM_R'	146	142	[12.2574324324324,-27.0554054054054,6.50810810810810]
'Thal_PuA_L'	147	143	[-12.3270676691729,-22.9962406015038,6.74060150375939]
'Thal_PuA_R'	148	144	[11.3175182481752,-21.8175182481752,6.62773722627738]
'Thal_PuL_L'	149	145	[-18.7196261682243,-25.4439252336449,10.4018691588785]
'Thal_PuL_R'	150	146	[16.2550000000000,-23.0800000000000,11.7750000000000]
'ACC_sub_L'	151	147	[-3.61727475800447,30.3760238272524,-5.99925539836188]
'ACC_sub_R'	152	148	[5.98484848484848,31.2878787878788,-4.92424242424242]
'ACC_pre_L'	153	149	[-4.46012759170654,43.1682615629984,6.71212121212122]
'ACC_pre_R'	154	150	[9.33333333333333,42.7716049382716,12.2283950617284]
'ACC_sup_L'	155	151	[-3.31487603305786,24.8024793388430,22.5611570247934]
'ACC_sup_R'	156	152	[8.39868667917449,27.0196998123827,20.6744840525328]
'N_Acc_L'	157	153	[-7.74171164225135,12.2737085582113,-7.73477255204318]
'N_Acc_R'	158	154	[10.2238055322716,12.4098910310142,-7.55993294216262]
'VTA_L'	159		[0,0,0]
'VTA_R'	160		[0,0,0]
'SN_pc_L'	161		[0,0,0]
'SN_pc_R'	162		[0,0,0]
'SN_pr_L'	163		[0,0,0]
'SN_pr_R'	164		[0,0,0]
'Red_N_L'	165		[0,0,0]
'Red_N_R'	166		[0,0,0]
'LC_L'	167		[0,0,0]
'LC_R'	168		[0,0,0]
'Raphe_D'	169	155	[0.628378378378372,-26.8783783783784,-10.3445945945946]
'Raphe_M'	170	156	[-0.0461538461538424,-30.0769230769231,-21.9538461538462]

In this context, brain regions labeled with coordinates [0,0,0] were considered as excluded regions. Out of the initial 170 brain regions, a total of 14 regions characterized by extremely low gray matter volumes were removed. Consequently, the analysis included a final set of 156 brain regions.

Table S5: the correlation of degree center and DBS improvement

	R-value	FDR p-value
lPreCG	-0.1790	0.0356
rMCC	0.2074	0.0147
lPHG	0.1904	0.0253
rPoCG	0.1809	0.0338
rSTG	-0.2225	0.0087
VER4_5	0.2170	0.0106
rtPuL	-0.2117	0.0127

Table S6: the correlation of local efficiency and DBS improvement

	R-value	FDR p-value
lHIP	-0.2500	0.0031
lPHG	0.1691	0.0475
rPHG	0.1754	0.0396
lIOG	-0.1792	0.0354
rIOG	-0.2380	0.0049

rPoCG	0.1920	0.0241
lSMG	0.1847	0.0301
rSTG	-0.1731	0.0424
lCER3	0.1812	0.0334
ltVPL	-0.2166	0.0107
rtPuL	-0.1697	0.0466
rRedN	-0.2302	0.0066